Soft Graphoepitaxy for Large Area Directed Self-Assembly of Polystyrene-*block*-Poly(dimethylsiloxane) Block Copolymer on Nanopatterned POSS Substrates Fabricated by Nanoimprint Lithography

Dipu Borah, Sozaraj Rasappa, Mathieu Salaun, Marc Zellsman, Olivier Lorret, George Liontos, Konstantinos Ntetsikas, Apostolos Avgeropoulos, and Michael A. Morris**

Polyhedral oligomeric silsequioxane (POSS) derivatives have been successfully employed as substrates for graphoepitaxial directed self-assembly (DSA) of block copolymers (BCPs). Tailored POSS materials of tuned surface chemistry are subject to nanoimprint lithography (NIL) resulting in topographically patterned substrates with dimensions commensurate with the BCP block length. A cylinder forming polystyrene-*block*-polydimethylsiloxane (PS-*b*-PDMS) BCP is synthesized by sequential living anionic polymerization of styrene and hexamethylcyclotrisiloxane. The patterned POSS materials provide a surface chemistry and topography for DSA of this BCP and after solvent annealing the BCP shows well-ordered microphase segregation. The orientation of the PDMS cylinders to the substrate plane could be controlled within the trench walls by the choice of the POSS materials. The BCP patterns are successfully used as on-chip etch mask to transfer the pattern to underlying silicon substrate. This soft graphoepitaxy method shows highly promising results as a means to generate lithographic quality patterns by nonconventional methods and could be applied to both hard and soft substrates. The methodology might have application in several fields including device and interconnect fabrication, nanoimprint lithography stamp production, nanofluidic devices, lab-on-chip, or in other technologies requiring simple nanodimensional patterns.

1. Introduction

The performance of semiconductor devices is dictated by the resolution of the lithographic process. To keep pace with historic growth rates (i.e., Moore's law), the dimensions of critical circuit elements are shrinking toward 10 nm. The success of micro- and nano- technology is dependent on its ability to fabricate these ultrasmall structures with high precision using techniques typified by projection lithography. Top-down lithographic techniques include UV,[1] thermal,[2] e-beam,[3,4] and X-ray[5] methodologies. There are alternative bottom-up approaches based on the hierarchical self-assembly of complex structures from molecular building blocks through molecular recognition and molecule–surface interactions.[6] There are advantages and drawbacks in both approaches. In top-down methodologies further downsizing is governed by issues such as light particle dimensions and thermal management. On the other hand, it is highly challenging to achieve long-range translational order and structural robustness of the fabricated systems with bottom-up approaches.[7–9]

Directed self-assembly (DSA) is a promising technique where a self-assembled pattern is guided by an external field. Graphoepitaxy is a form of DSA where surface topography ordains pattern alignment and orientation.[10–13] Nanoimprint lithography (NIL)[14–16] is a technique that can be implemented for the simple generation of topography for block copolymer (BCP) DSA.[14,17,18] Direct NIL of a BCP film was first reported by Li and Huck[19] on polystyrene-*block*-polymethylmethacrylate (PS-*b*-PMMA).

Dr. D. Borah, Dr. S. Rasappa, Prof. M. A. Morris
Department of Chemistry
University College Cork
Cork, Ireland
E-mail: d.borah@ucc.ie; m.morris@ucc.ie
Dr. D. Borah, Dr. S. Rasappa, Prof. M. A. Morris
Tyndall National Institute
Lee Maltings, Prospect Row, Cork, Ireland
Dr. D. Borah, Dr. S. Rasappa, Prof. M. A. Morris
Centre for Research on Adaptive Nanostructures and Nanodevices (CRANN)
Trinity College Dublin
Dublin 2, Ireland
Dr. M. Salaun, Dr. M. Zellsman
Laboratoire des Technologies de la Microelectronique (CNRS)
38054 Grenoble, France
Dr. O. Lorret
Profactor GmbH
Functional Surfaces and Nanostructures
4407 Steyr-Gleink, Austria
Dr. G. Liontos, Dr. K. Ntetsikas, Prof. A. Avgeropoulos
Department of Materials Science Engineering
University of Ioannina
University Campus-Dourouti
45110 Ioannina, Greece

DOI: 10.1002/adfm.201500100

PS-*b*-PMMA is advantageous in that it is consistent with manufacturing processes.[20–22] Under suitable self-assembly conditions, lamellar or cylindrical structures can be obtained on the surface with pitches varying from 35 to 50 nm. However, the Flory–Huggins parameter is relatively low that limits the smallest feature size attainable. Other BCPs, for example, polystyrene-*block*-polyethyleneoxide (PS-*b*-PEO)[23] and polystyrene-*block*-poly(lactide) (PS-*b*-PLA) have pitch sizes around 20 nm.[24] Currently, one of them most exciting systems is polystyrene-*block*-poly(dimethylsiloxane) (PS-*b*-PDMS) with sub-20 nm feature sizes reported recently by Park et al.,[25] employing NIL-assisted DSA. This BCP is very promising since its Flory–Huggins parameter ($\chi = 68/T - 0.037$) is relatively high allowing further pitch size reductions.[26] However, in PS-*b*-PDMS two major issues exist: strong dewetting from substrates due to high hydrophobicity and the difficulty in controlling feature orientation. To overcome these limitations, a surface pretreatment with a hydroxyl-terminated poly(dimethylsiloxane) (PDMS-OH) brush is usually required.[27–31]

Despite progress in the use of PS-*b*-PDMS, a method for precise control of surface wetting and pattern orientation remains a challenge, particularly for large substrate areas. A potential solution to control the surface chemistry and provide a platform for NIL-based graphoepitaxy is to use a resist that can be finely tuned to control surface chemistry and is photosensitive to provide NIL defined topography. Photosensitivity is important so that the NIL printed films are physically and chemically (since BCPs will be deposited by the solvent) robust. In the present work, two polyhedral oligomeric silsesquioxanes (POSS) derivatives with different surface chemistry were developed as UV-NIL resists. The use of these to generate highly periodic patterns and as on-chip etch masks is demonstrated.

2. Results and Discussion

Figure 1a,b shows the BCP pattern formed on the brush coated substrate as revealed by SEM. The formation of oxidized PDMS cylinders during this etch process is confirmed by FTIR from a Si—O—Si signal at 1100 cm^{-1}[32] as seen in Figure 1c. The optical image in Figure 1a reveals significant levels of dewetting of the BCP film after the solvent anneal resulting in a hill and valley structure (the film is smooth and of regular thickness prior to the solvent anneal). This leads to poor coverage (≈60% of the substrate), multilayer pattern formation, lower correlation length of PDMS cylinders, and macroscopic defects such as disclinations, dislocations, etc. The FIB cross-section SEM image in Figure 1b clearly shows the multilayer stacking of cylinders and suggests that ordering occurs in the in-plane and out-of-plane directions. The images also reveal the presence

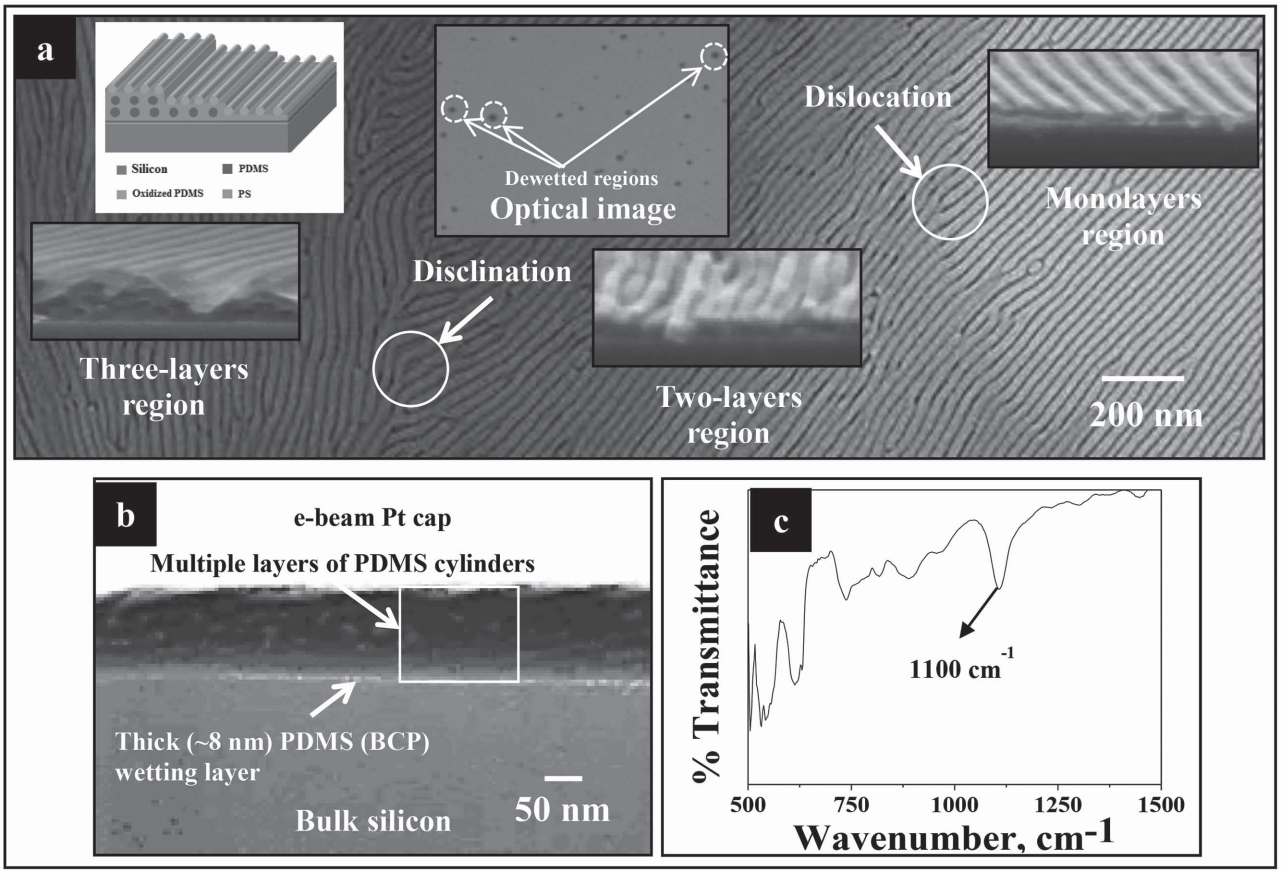

Figure 1. a) Top-down SEM image of PS-*b*-PDMS patterns at a PDMS-OH polymer brush modified substrate (after **ETCH1**). Insets in (a) are cross-section SEM images of monolayer and multilayers of PDMS cylinders, a schematic, and an optical image of the BCP film after solvent annealing. b) FIB cross-section SEM image of etched PS-*b*-PDMS films demonstrating multiple layers of PDMS cylinders in thicker dewetted regions of (a). c) FTIR spectrum of a similar sample.

Table 1. Contact angle (θ) and surface free energy (SFE) of POSS-A and POSS-G.

POSS type	θ_{DI} [°]	θ_{DIM} [°]	θ_{EG} [°]	SFE [mN m^{-1}]
POSS-A	59.3	42.7	33.9	47.5
POSS-G	68.1	43.0	44.9	42.7

of the expected wetting PDMS layer of ≈8 nm unaffected by **ETCH1**. The presence of the wetting layer suggests a strong PDMS (brush)– PDMS (BCP) interaction exists. The mean PDMS L_0 (cylinder-to-cylinder spacing) and cylinder <*d*> are 63.5 nm and 31.8 nm, respectively.

POSS materials can control the surface chemistry and be used as an alternative to standard polymer brushes for BCP ordering.[21,33,34] The properties of the POSS materials can be varied by grafting different ligands to the POSS cages as is revealed from the data compiled in **Table 1** for POSS-A and POSS-G that are functionalized with eight aliphatic acrylo and glycidyl groups, respectively. The structural formulae of the POSS derivatives are presented in **Scheme 1**. It is evident from Table 1 that POSS-A has a lower water contact angle as well as higher surface free energy after polymerization and the reverse is true for POSS-G. The surface free energies of PS and PDMS are 29.9 and 19.8 mN m^{-1}, respectively.[35,36] A comparison of the surface free energies of POSS-A and POSS-G with that of PDMS reveals that the POSS derivatives have higher surface free energies. According to Harrison et al.,[37] a polymer brush made of the minority block (PDMS here) that preferentially wets the substrate is likely to have little effect on ordering of the BCP. Thus, the POSSs substrates with higher surface free energy seems to provide the perfect energy barrier for the diffusion of PS-*b*-PDMS BCP into the resist surface.

Self-assembly of the PS-*b*-PDMS BCP on planer POSS coated substrates is presented in **Figure 2**. The SEM data for both POSS-A and POSS-G coatings suggest that the wetting properties of the BCP improve substantially (more than 90% coverage of a film of uniform film thickness) when compared to the PDMS-OH functionalized substrates described above. A further advantage of using POSS coatings avoids the need for the very lengthy brush deposition step. Distinct differences were seen between the POSS types. For POSS-G, the pattern displays a consistent parallel (to the surface plane) arrangement of cylinders, whilst POSS-A presents a mixture of complex morphologies. In regions of the POSS-A substrate regular cylinder patterns and a hexagonal arrangement of hemisphere can be seen. An unusual structure of sphere-supported cylinders creating a net-like structure was also formed suggesting a perforated lamellar structure or similar.[38] These differing morphologies indicate that subtle changes in surface energy can have dramatic effects on the lowest energy conformation and it is clear that the effective composition of the microphase separated region of the BCP pattern is altered by segregation to interfaces. It should be noted that POSSs being silicon-based compounds, it might preferentially wet the PDMS block of the BCP forming a PDMS wetting layer at the BCP–POSS interface. However, it is very difficult to isolate the PDMS wetting layer from the POSS resist in the cross-section SEM images because of the similar contrast. For the parallel cylinder arrangement (both POSS-A and POSS-G, the PDMS L_0 and <*d*> values are ≈63.5 and ≈31.8 nm (in agreement with the measurements at the PDMS-OH brush surface). For the spherical morphology, the periodicity and the PDMS sphere dimension are ≈79.4 and ≈35.2 nm, respectively. It can be seen from the figure that the in-plane PDMS cylinders exhibit a greater degree of alignment on POSS-G compared to POSS-A that probably arises from the structural instability noted above.

Whilst the POSS-coated surfaces improve BCP deposition (see above), they also form the topography for DSA via NIL. These topographically patterned surfaces are also useful in understanding the changes in surface chemistry that results from functionalization since assembly at the sidewall can be readily imaged. It was also found useful to study differences in patterns as a function of the residual layer being present or not before application of the BCP. It was reported that the deposited POSS layers can be uniformly imprinted over the 4 in. substrate with very low macroscopic and microscopic defect densities.[33] An optical microscopy image of the imprinted POSS substrate is presented in Figure S1 (Supporting Information). The NIL patterns (50 nm deep 270 nm wide channels, 500 nm pitch) are of good quality (both before and after residual resist layer removal). Note that the trench width is close to commensurate with four pitches (4 × 63.5 nm) of the BCP used.

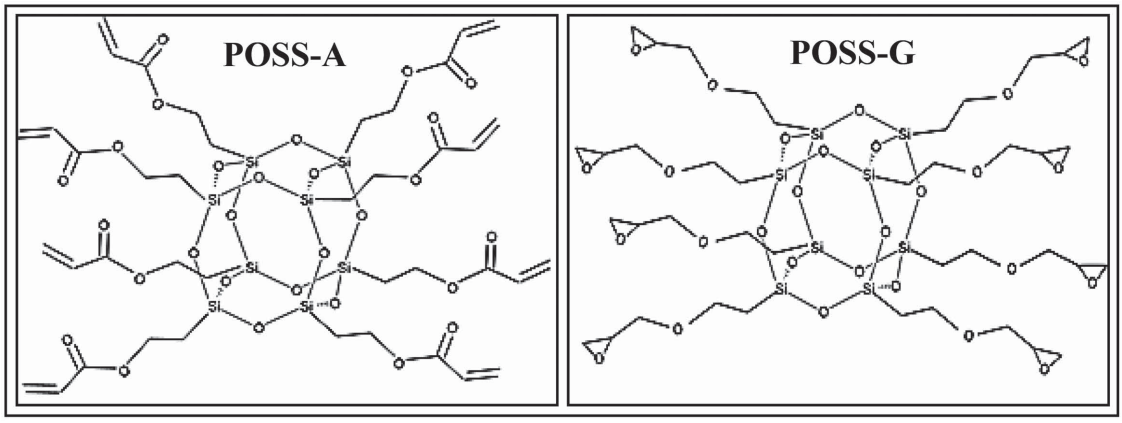

Scheme 1. Structural details of the POSS resists used in the present study.

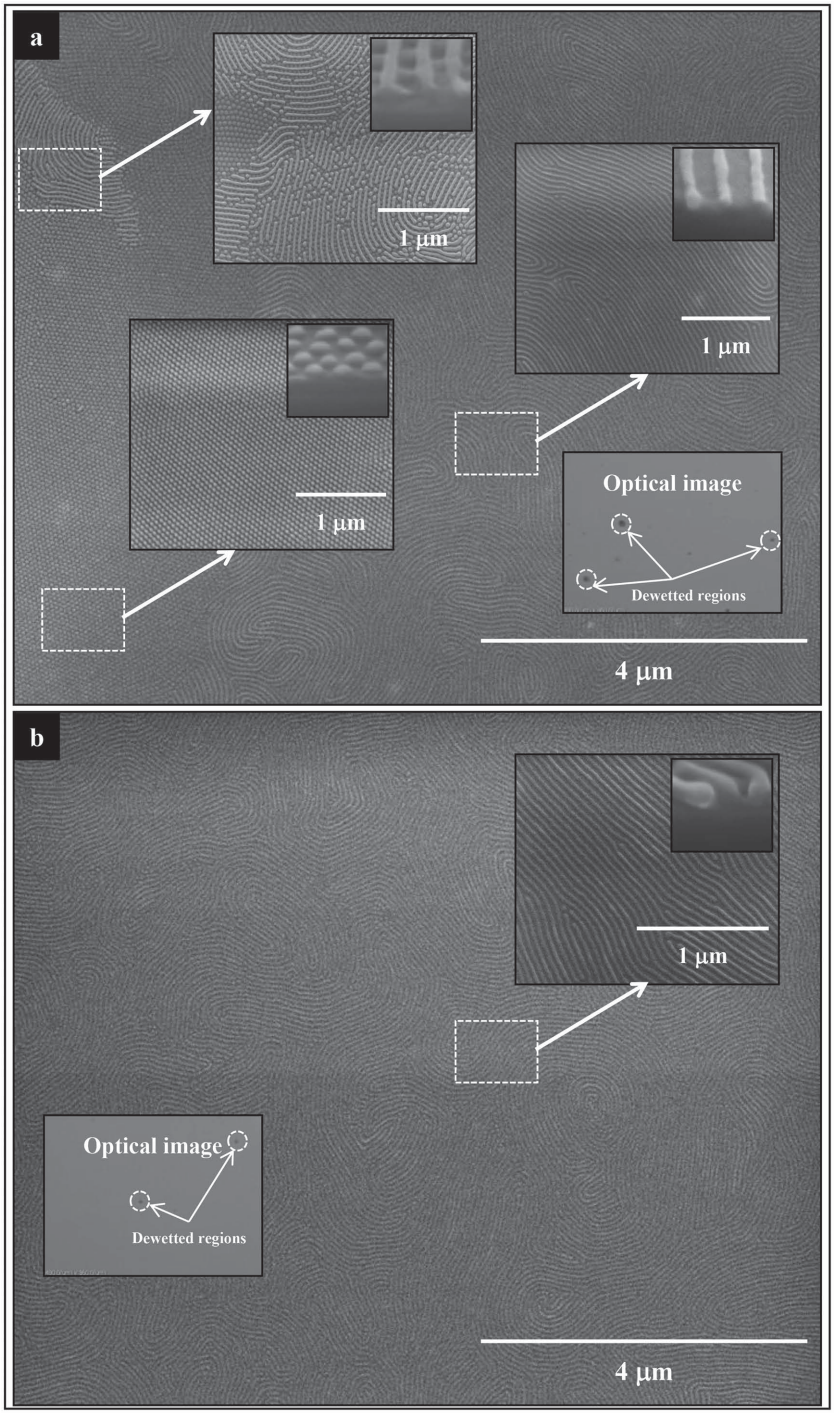

Figure 2. SEM images of PS-*b*-PDMS derived structures at planer substrates coated with a) POSS-A and b) POSS-G after **ETCH1**. Insets are higher resolution SEM images of specific sections and optical images of the BCP films after solvent anneal.

Figures 3 and **4** show PS-*b*-PDMS patterns (after **ETCH1**) following solvent annealing. Both POSS derivatives are compatible with graphoepitaxial DSA of the PS-*b*-PDMS system. With the resist layer present (Figure 3), highly ordered parallel cylinder arrangements are observed. This is expected since both POSSs favored this orientation of cylinders and the sidewalls will act so as to direct the horizontal alignment. Note that the sidewalls remove the tendency to produce mixed morphologies for POSS-G presumably because of the additional structural directing power of the topography. On similar substrates where the residual layer has been removed, the hexagonal cylinder arrangement switches orientation to perpendicular for both substrate types (Figure 4). This suggests that the substrate surface is somewhat "neutral" to the blocks so both wet the surface equally. It should be noted that the degree of order for the parallel arrangement is much better than for the hexagonal arrangement. This may simply reflect the lower symmetry and greater degree of structural freedom. Indeed, most of the structural imperfections in the vertical orientation arise from rotational errors. It should also be noted that the vertically orientated hexagonal pattern on POSS-G has significantly greater order than that on POSS-A.

The usefulness of the cylinder forming PS-*b*-PDMS system for nanofabrication was demonstrated by applying a plasma etch procedure for pattern transfer (**ETCH 2**) followed by the removal of the residual oxidized PDMS cylinders and the remaining PS matrix (**ETCH3**). **Figure 5** shows the SEM images of the silicon nanopillars/wires formed. Essentially, oxidized PDMS structures are used as a hard mask (highly etch resistant) for pattern transfer to the surface. During this oxidation, special care is required to minimize the undercut of the PDMS cylinders that can lead to poor quality pattern transfer. The high-resolution cross-section SEM images of the silicon transferred features derived from the vertically orientated PS-*b*-PDMS patterns on POSS-A (after stripping of the residual resist layer) reveal well-ordered cylinder structures. The cylinders have a diameter and height of ≈24.5 nm and ≈49 nm, respectively. It should be noted that the POSS-A mesa is also affected by the etch treatments producing significant reduction in sidewall height (reduced to ≈20 nm from the original 50 nm) and a roughened surface so that the top of the nanopillars is above the NIL patterned trenches. This is consistent with lower etch resistance of the POSS. Note that very similar results were seen with patterns formed at POSS-G coated substrates.

However, pattern transfer of the in-plane cylindrical PDMS patterns on POSS-A (residual layer present) did not result in such well-defined silicon nanofeatures as shown in Figure 5. The high-resolution cross-section SEM image shows that the expected silicon nanowires are broken. The mesa is similarly effected to that seen above for the vertical orientation. Similar

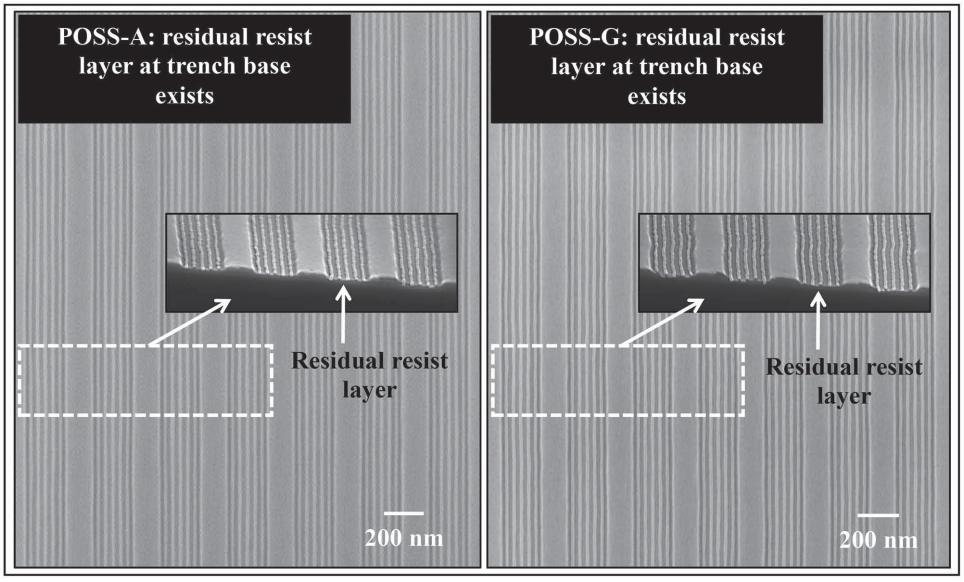

Figure 3. Top-down and cross-section (insets) SEM images of cylinder-forming PS-*b*-PDMS derived structures at nanopatterned POSS substrates with the residual resist layer remaining at the channel base. The silicon substrates were coated with two different POSS materials as labeled in the images.

results were seen with patterns formed at POSS-G coated substrates. The nonideal nature of the pattern transfer process can be assigned to two reasons both related to the relatively poor etch contrast between silica and silicon, which suggests that thicker hard mask features are required. First, for the vertical arrangement, **ETCH1** results in a silica-like that mimics the BCP arrangement, but the cylinders extended through the film thickness resulting in a significant thickness of the silica hard mask. For the parallel arrangement, the effective thickness is reduced because the silica hard mask thickness is related to the cylinder dimension not the film thickness. This will also result in a thickness profile across the line being thickest at the center and this might explain the thinness of the silicon structures observed. The second reason for poor pattern transfer might be the formation of a wetting layer. For the vertical orientation, the surface is seen to be neutral and no PDMS wetting layer would be expected. A wetting layer of PDMS would result in a silica-like film of significant thickness that would hinder selectivity. For the parallel arrangement, the POSS residual layer might be expected to favor a PDMS wetting layer. In this way, in the parallel arrangement, a rather thin hard mask layer sits on another hard mask layer and etch differentiation is compromised. This might suggest that the etch processes need careful optimization or alternative etch chemistries found.

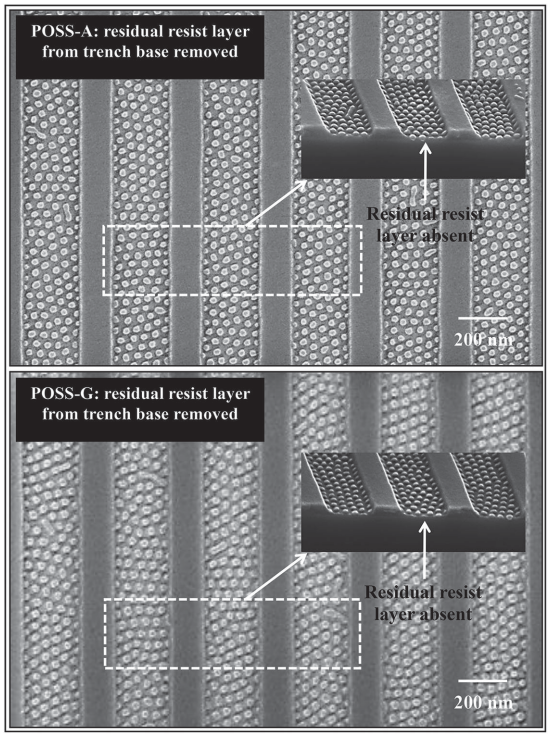

Figure 4. Top-down and cross-section (insets) SEM images of cylinder forming PS-*b*-PDMS derived structures at nanopatterned POSS substrates with residual resist layer removed. The silicon substrates were coated with two different POSS materials as labeled in the images.

3. Conclusions

In summary, a methodology for producing highly ordered silicon nanofeatures at a substrate has been detailed using NIL imprinted substrates for graphoepitaxy. An integrated approach to nanofabrication has been developed and shown to be highly effective and, we assert, represents a major breakthrough in the nanofabrication process. The use of POSS films allows control of pattern orientation and alignment to generate silicon nanowire and cylinder structures. Orientation is controlled through the removal or retention of the NIL residual layer. This holds much promise as a fabrication method since selected area removal can allow formation of both nanopillars and nanowire structures at the same substrate. The ability to ''tune'' the surface chemistry of the POSS resist structures allows optimization of chemistry and therefore, ordains highly

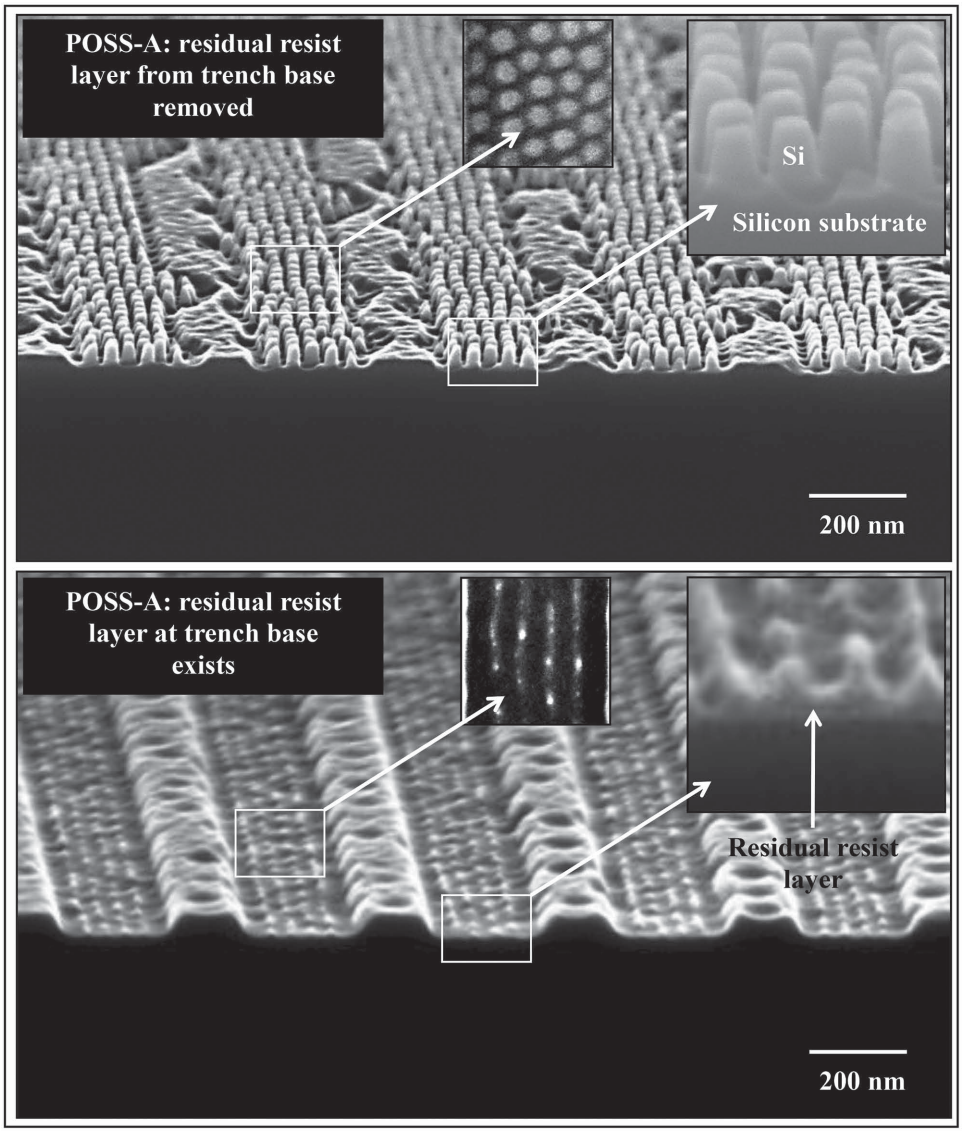

Figure 5. Tilted (25°) SEM images of PDMS patterns transferred to form silicon features on substrates (POSS-A substrates). Data labeled in the figure. Insets show high-resolution top-down and cross-section SEM images of specific sections.

regular arrangements. Note that although we have used NIL for convenience here, these and similar materials are amenable to conventional 193 nm UV lithography.

4. Experimental Section

Synthesis of Polymers: The PS-*b*-PDMS BCP was synthesized by sequential living anionic polymerization of styrene and hexamethylcyclotrisiloxane (D_3), employing high vacuum techniques as described in the Supporting Information. The number average molecular weights (M_n) per block and polydispersity index (M_w/M_n) of the BCP were determined using membrane osmometry (MO) and size exclusion chromatography (SEC) experiments leading to values: M_n^{PS} = 53.0 kg mol^{-1}, M_n^{PDMS} = 17.0 kg mol^{-1}, and M_w/M_n = 1.07. The volume fraction (ϕ_{ps}) of PS in the BCP was calculated by ^{1}H-nuclear magnetic resonance (NMR) spectroscopy equal to 0.72. The hydroxyl-terminated PDMS (PDMS-OH) polymer brush was synthesized by living anionic polymerization of hexamethylcyclotrisiloxane (D_3) with sec-BuLi as an initiator, end capped with one to two monomeric units of ethylene oxide (EO) in pyridine and terminated with methanol (MeOH). The number average molecular weight (M_n) and polydispersity (M_w/M_n) of the PDMS-OH were determined by the MO and SEC techniques equal to: M_n^{PDMS} = 5.5 kg mol^{-1} and M_w/M_n = 1.06, respectively. The molecular characterization results from SEC, MO, and ^{1}H-NMR for the two polymers (BCP and PDMS-OH) indicated molecular and compositional homogeneity. The potential for microphase separation of the BCP was indicated by differential scanning calorimetry (DSC) and the results exhibited two distinctive glass transition temperatures: T_{g1} = ≈150.74 K (–122.41 °C) and T_{g2} = ≈375.35 K (102.02 °C), corresponding to nonmiscible PDMS and PS macromolecular chains, respectively. The details of molecular characterization are available in the Supporting Information.

POSS Materials and Substrate Fabrication by UV-NIL: Acrylo POSS (POSS-A) and Glycidyl POSS (POSS-G) were purchased from Hybrid Plastics. Ethyl-L-lactate was purchased from Sigma-Aldrich. The photoinitiators Irgacure 250 (iodonium (4-methylphenyl)

[4-(2-methylpropyl) phenyl]-hexafluorophosphonate, 75 wt% in propylene carbonate), and the sensitizer Genocure isopropyl thioxanthone (ITX) were generously provided by BASF Resins and RAHN AG Energy Curing, respectively. POSS monomers were diluted in propylene glycol methyl ether acetate (PGMEA). 2 mol% (relative to epoxy groups) of Irgacure 250 (photo-initiator absorbing in the range 275–325 nm in wavelength) and 0.5 wt% of Genocure ITX (sensitizer absorbing in the range 340–400 nm) were added to the solutions to provide UV sensitivity. These solutions were spin coated onto 4 in. silicon wafers (<100> orientation, B-doped, p-type, thickness 650 μm, and resistivity 6–14 Ω cm) with a native oxide layer of ≈2 nm to form a 50 nm thick resist film. Some non-NIL patterned POSS coated substrates were retained to study microphase separation on planer surfaces. Topographical graphoepitaxial substrates were fabricated using UV nanoimprint lithography with an elastomeric mold (so-called "soft UV NIL") in the POSS resists. A PDMS mold (so as to form 50 nm deep, 270 nm wide trenches in the resist) was repeatedly stamped over the substrate (full coverage) at a pressure of 200 kPa and exposed to UV radiation (365 nm in wavelength) for 3 min to cure the resist. Prior to imprinting, molds were treated with an anti-sticking layer (Optool DSX, Daikin chemical) based on fluorosilanes. This layer had a thickness of about 3 nm and resulted in a surface free energy of 110.5 mN m^{-1} for even demolding. The process formed a resist residual layer at the bottom of each of the topographically patterned trenches (≈15 nm thick) that could be removed by CF_4 (15 sccm) plasma for 4–8 s (determined by the resist time) with an inductively coupled plasma (ICP) and reactive ion etching (RIE) powers of 400 W and 30 W, respectively, at 2.0 Pa with a helium backside cooling pressure of 1333.2 Pa. This resulted in 45 nm deep trenches consisting of a silicon bottom and POSS resist sidewalls.

Deposition of PDMS-OH Brush on the Substrate: The substrates were cut into 2.0 cm^2 pieces and degreased by ultrasonication in acetone and IPA solutions for 5 min each, dried in flowing N_2 gas and baked for 2 min at 393 K in an ambient atmosphere to remove any residual IPA. This was followed by cleaning in a piranha solution (1:3 v/v 30% H_2O_2:H_2SO_4) at 363 K for 60 min, rinsed with DI water (resistivity ≥ 18 MΩ cm^{-1}) several times, acetone, ethanol, and dried under N_2 flow. Piranha activation removed any organic contaminant, greased, and created silanol groups on the silicon substrates. The hydroxyl-terminated PDMS brush solution of 1.0 wt% in toluene was spin-coated (P6700 Series Spin-Coater, Speciality Coating Systems) onto silicon wafers at 3000 rpm for 30 s. Samples were annealed in a vacuum oven (Townson and Mercer EV018) at 443 K under vacuum (1.3 kPa of residual pressure) for 6 h. This allowed the end-functional hydroxyl groups of the homopolymer to bond to the silanol groups and chemically anchor the brush to the substrate. Unbound polymers were removed by sonication (Cole-Palmer 8891 sonicator) and rinsing in toluene.

Deposition of PS-b-PDMS and Solvent Annealing: Thin films of PS-*b*-PDMS were prepared by depositing dilute solution (1.0 wt%) of the diblock copolymer in toluene onto polymer brush anchored planner silicon, and unpatterned/patterned POSS substrates by spin coating (as above). As-cast thin films were solvent annealed in glass jars under saturated toluene environment at room temperature (≈288 K) for 3 h. Samples were removed from the glass jars after the desired anneal time and allowed to evaporate the trapped solvent under ambient conditions.

Plasma Etching of PS-b-PDMS Films and Pattern Transfer: Following BCP film formation, atomic force microscopy could not readily show the microphase-separated structure because of the presence of a surface-wetting layer of PDMS that must be removed to reveal the BCP arrangement.[27–31] A multistep etch process (**ETCH1**) was developed to reveal the pattern. Solvent-annealed PS-*b*-PDMS films were etched in CF_4 to remove the surface PDMS layer. This was followed by an O_2 plasma treatment to remove exposed PS component and oxidize the PDMS cylinders. These steps followed a similar methodology developed by Ross and Jung.[31] The oxidized PDMS cylinders were then used as an etch mask for pattern transfer (i.e., **ETCH2**) to silicon. The first part of the process was a CHF_3/Ar plasma etch to remove exposed passive silica layer or PDMS between the PDMS **ETCH1** derived cylinders. This was followed by a selective silicon etch using CHF_3 and SF_6 to transfer the cylinder patterns into the underlying substrate. Any residual carbon polymer materials were removed by a CHF_3/Ar etch. This was followed by an O_2 etch to remove residual PS (**ETCH3**). Full etch details are given elsewhere.[28,39] The POSS template fabrication process and the subsequent BCP self-assembly and plasma etching are outlined in **Scheme 2**.

Material Analysis: Contact angles and surface free energy measurements were carried out using a Krüss DSA 100 goniometer. Contact angles were measured by the static sessile drop method, surface free energy was calculated from the measured contact angles of deionized water (DI), diiodomethane (DIM) and ethylene glycol (EG) using the Owens–Wendt model.[40] Film thickness was determined by ellipsometry (Plasmos SD2000 Ellipsometer) at an incidence angle of 70° and five measurements from different locations were used to estimate the thickness. An IR660, Varian infrared spectrometer was used to record FTIR spectra. The measurements were performed in the spectral range of 4000–500 cm^{-1}, with a resolution of 4 cm^{-1} and data averaged over 32 scans. Optical micrographs of POSS templates were from a Nikon Optiphot microscope with a 40× power long-working distance objective. Surface morphology and silicon nanostructures were investigated by scanning electron microscopy using a high-resolution (<1 nm) Field Emission Zeiss Ultra Plus-SEM with a Gemini column operating at an accelerating voltage of 5 kV. Cross-sections were also used to estimate film thickness and were in good agreement with ellipsometry. An FEI Strata 235-Focused Ion Beam (FIB) tool with a resolution of 10 nm was used for cross-sectional analysis. E-beam platinum was deposited onto patterns followed by ion-beam platinum. Milling and polishing of the protective coatings was performed at the lower aperture size and the specimen was imaged under the higher resolution Zeiss Ultra Plus-SEM.

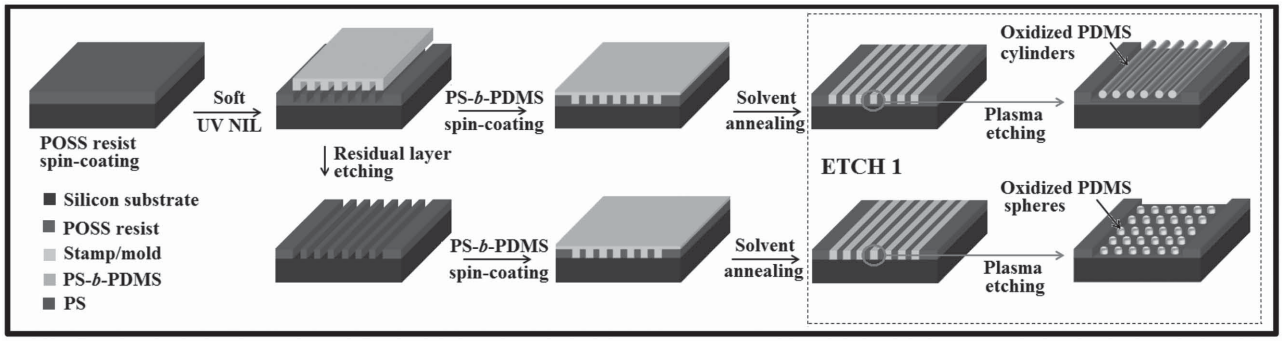

Scheme 2. Schematic depicting fabrication of the nanopatterned POSS template, PS-*b*-PDMS self-assembly, and **ETCH1**, as described in the text and the figure.

Supporting Information

Supporting Information is available from the Wiley Online Library or from the author.

Acknowledgements

Financial support for this work was provided by the EU FP7 NMP Project, LAMAND (Grant Number 245565) Project and the Science Foundation Ireland (Grant Number 09/IN.1/602), and gratefully acknowledged.

Received: January 9, 2015
Revised: March 22, 2015
Published online: April 27, 2015

[1] M. Wissen, N. Bogdanski, S. Moellenbeck, H. C. Scheer, in *24th European Mask and Lithography Conf., Proceedings of SPIE Vol. 6792* (Ed. Uwe F. W. Behringer), SPIE, Bellingham, WA, USA **2008**, V7920.
[2] S. Chung, J. R. Felts, D. Wang, W. P. King, J. J. De Yoreo, *Appl. Phys. Lett.* **2011**, *99*, 193101.
[3] A. E. Grigorescu, C. W. Hagen, *Nanotechnology* **2009**, *20*, 292001.
[4] H. Namatsu, Y. Watanabe, K. Yamazaki, T. Yamaguchi, M. Nagase, Y. Ono, A. Fujiwara, S. Horiguchi, *J. Vac. Sci. Technol. B* **2003**, *21*, 1.
[5] Y. Hirai, S. Hafizovic, N. Matsuzuka, J. G. Korvink, O. Tabata, *J. Microelectromech. Syst.* **2006**, *15*, 159.
[6] I. W. Hamley, *Angew. Chem. Int. Ed.* **2003**, *42*, 1692.
[7] P. Kumar, *Nanoscale Res. Lett.* **2010**, *5*, 1367.
[8] K. Ariga, J. P. Hill, M. V. Lee, A. Vinu, R. Charvet, S. Acharya, *Sci. Technol. Adv. Mater.* **2008**, *9*, 014109.
[9] C. J. Hawker, T. P. Russell, *MRS Bull.* **2005**, *30*, 952.
[10] M. Takenaka, H. Hasegawa, *Curr. Opin. Chem. Eng.* **2013**, *2*, 88.
[11] J. Bang, U. Jeong, D. Y. Ryu, T. P. Russell, C. J. Hawker, *Adv. Mater.* **2009**, *21*, 4769.
[12] I. W. Hamley, *Prog. Polym. Sci.* **2009**, *34*, 1161.
[13] R. A. Segalman, *Mater. Sci. Eng., R* **2005**, *48*, 191.
[14] L. J. Guo, *Adv. Mater.* **2007**, *19*, 495.
[15] M. D. Austin, H. Ge, W. Wu, M. Li, Z. Yu, D. Wasserman, S. A. Lyon, S. Y. Chou, *Appl. Phys. Lett.* **2004**, *84*, 5299.
[16] C. Acikgoz, M. A. Hempenius, J. Huskens, G. J. Vancso, *Eur. Polym. J.* **2011**, *47*, 2033.
[17] B. D. Gates, Q. Xu, M. Stewart, D. Ryan, C. G. Willson, G. M. Whitesides, *Chem. Rev.* **2005**, *105*, 1171.
[18] T. Mårtensson, P. Carlberg, M. Borgström, L. Montelius, W. Seifert, L. Samuelson, *Nano Lett.* **2004**, *4*, 699.
[19] H.-W. Li, W. T. S. Huck, *Nano Lett.* **2004**, *4*, 1633.
[20] D. Borah, M. T. Shaw, S. Rasappa, R. A. Farrell, C. T. O'Mahony, C. M. Faulkner, M. Bosea, P. Gleeson, J. D. Holmes, M. A. Morris, *J. Phys. D: Appl. Phys.* **2011**, *44*, 174012.
[21] R. A. Farrell, N. Kehagias, M. T. Shaw, V. Reboud, M. Zelsmann, J. D. Holmes, C. M. Sotomayor Torres, M. A. Morris, *ACS Nano* **2011**, *5*, 1073.
[22] M. Salaün, N. Kehagias, B. Salhi, T. Baron, J. Boussey, C. M. Sotomayor Torres, M. Zelsmann, *J. Vac. Sci. Technol. B* **2011**, *29*, 06F208.
[23] T. H. Kim, J. Hwang, H. Acharya, C. Park, *J. Nanosci. Nanotechnol.* **2010**, *10*, 6883.
[24] M. Vayer, M. A. Hillmyer, M. Dirany, G. Thevenin, R. Erre, C. Sinturel, *Thin Solid Films* **2010**, *518*, 3710.
[25] S. M. Park, X. Liang, B. D. Harteneck, T. E. Pick, N. Hiroshiba, Y. Wu, B. A. Helms, D. L. Olynick, *ACS Nano* **2011**, *5*, 8523.
[26] N. Politakos, E. Ntoukas, A. Avgeropoulos, V. Krikorian, B. D. Pate, E. L. Thomas, R. M. Hill, *J. Polym. Sci., Part B: Polym. Phys.* **2009**, *47*, 2419.
[27] D. Borah, M. T. Shaw, J. D. Holmes, M. A. Morris, *ACS Appl. Mater. Interfaces* **2013**, *5*, 2004.
[28] D. Borah, S. Rasappa, R. Senthamaraikannan, B. Kosmala, M. T. Shaw, J. D. Holmes, M. A. Morris, *ACS Appl. Mater. Interfaces* **2013**, *5*, 88.
[29] D. Borah, M. Ozmen, S. Rasappa, M. T. Shaw, J. D. Holmes, M. A. Morris, *Langmuir* **2013**, *29*, 2809.
[30] R. G. Hobbs, R. A. Farrell, C. T. Bolger, R. A. Kelly, M. A. Morris, N. Petkov, J. D. Holmes, *ACS Appl. Mater. Interfaces* **2012**, *4*, 4637.
[31] Y. S. Jung, C. A. Ross, *Nano Lett.* **2007**, *7*, 2046.
[32] C. T. Kirk, *Phys. Rev. B: Condens. Matter* **1998**, *38*, 1255.
[33] S. Mathieu, M. Zelsmann, S. Archambault, D. Borah, N. Kehagias, C. Simao, O. Lorret, M. T. Shaw, C. Sotomayor Torres, M. A. Morris, *J. Mater. Chem. C* **2013**, *1*, 3544.
[34] C. Simao, A. Francone, D. Borah, O. Lorret, M. Salaun, B. Kosmala, M. T. Shaw, B. Dittert, N. Kehagias, M. Zelsmann, M. A. Morris, C. M. Sotomayor Torres, *J. Photopolym. Sci. Technol.* **2012**, *25*, 239.
[35] D. A. Winesett, S. Story, J. Luning, H. Ade, *Langmuir* **2003**, *19*, 8526.
[36] M. Bračič, T. Mohan, R. Kargl, T. Griesser, S. Hribernik, S. Köstler, K. Stana-Kleinschek, L. Fras-Zemljič, *RSC Adv.* **2014**, *4*, 11955.
[37] C. Harrison, P. M. Chaikin, D. A. Huse, R. A. Register, D. H. Adamson, A. Daniel, E. Huang, P. Mansky, T. P. Russell, C. J. Hawker, D. A. Egolf, I. V. Melnikov, E. Bodenschatz, *Macromolecules* **2000**, *33*, 857.
[38] Y. S. Jung, C. A. Ross, *Adv. Mater.* **2009**, *21*, 2540.
[39] D. Borah, R. Senthamaraikannan, S. Rasappa, B. Kosmala, J. D. Holmes, M. A. Morris, *ACS Nano* **2013**, *7*, 6583.
[40] M. Zenkiewicz, *Polym. Test* **2007**, *26*, 14.